Exploring the interaction of alkali metal cations with the tetramethylborate anion

Lucía Vidal,[a,b] Jorge Gonzalo,[b] Noushin Keshtkar,[a] Víctor Polo,[b,c] Julen Munárriz,[b,c] and Jorge Echeverría[a]*

[a]Instituto de Síntesis Química y Catalisis Homogénea (ISQCH) and Department of Inorganic Chemistry, Facultad de Ciencias, Universidad de Zaragoza, Pedro Cerbuna 12, 50009 Zaragoza, Spain.
[b]Departamento de Química Física, Facultad de Ciencias, Universidad de Zaragoza, Pedro Cerbuna 12, 50009 Zaragoza, Spain
[c]Instituto de Biocomputación y Física de Sistemas Complejos (BIFI), Universidad de Zaragoza, 50009 Zaragoza, Spain

e-mail: jorge.echeverria@unizar.es

ABSTRACT

Understanding the interactions between metallic cations and anions is crucial for elucidating the structure and reactivity of ionic systems. In this work, we investigate the binding modes and energetic characteristics of a series of alkali metal cations (Li^+, Na^+, K^+, Rb^+, Cs^+) with the tetramethylborate anion using density functional theory. Molecular electrostatic potential analysis reveals three preferential binding regions corresponding to distinct local minima on the tetramethylborate surface. Geometry optimizations and penetration index analysis confirm the formation of ion pairs with site-specific interaction modes: κ^1C, κ^2C, and κ^1B. Energy decomposition analysis shows that electrostatics dominates the interaction energy, with polarization playing a significant secondary role. Correlations between penetration indices and interaction energies provide insight into the nature of cation–anion interactions, including the role of collective stabilization effects. These findings contribute to a deeper understanding of ion pairing phenomena in organoborate-based systems and the broader field of supramolecular chemistry.

Keywords: tetramethylborate; noncovalent interactions; ion pairs; penetration index.

INTRODUCTION

Understanding how cations and anions interact is fundamental to nearly every field of chemistry, from inorganic coordination chemistry to materials science and biochemistry. These interactions, which are mainly electrostatic and often directional, affect the stability, solubility, reactivity, and structure of many chemical systems. In solution chemistry, ion pairing can significantly influence both the rate at which reactions occur and how they reach equilibrium.[1] In solid-state chemistry, the way ions are arranged determines the structure of crystals and their properties, like conductivity and magnetism.[2] Ionic interactions are also key for enzyme function, membrane potential regulation, and molecular recognition in biological systems.[3] Chemists can rationally design new compounds, optimize reaction conditions, and create functional materials with specific properties by having a deep understanding of how certain cations and anions interact with each other, both on their own and in complex matrices.[4]

Among the various borate-based anions, the tetramethylborate anion (TMB), $[B(CH_3)_4]^-$, is of particular interest due to its compact geometry, disperse electron-rich nature, and potential to engage in weak but structurally significant interactions with a variety of metal centers. Despite its relevance in organoboron and ionic liquid chemistry, detailed studies on its coordination behavior and binding characteristics with metallic cations remain limited.[5, 6] Most of the current literature on borate–metal interactions focuses on more complex or reactive borate species, such as tetrafluoroborate (BF_4^-)[7, 8] or tetrahydroborate (BH_4^-),[9, 10] which are well known for their roles in coordination compounds and reduction chemistry. In contrast, the TMB anion, with its larger size, sterically hindering methyl substituents, and relative chemical inertness, serves as a distinctive model for exploring non-covalent cation–anion interactions in the solid state.

In this work, we systematically explore the interaction between various metallic cations, namely alkali metals, and the TMB anion using a combination of computational techniques. By comparing trends across different cationic species, we aim to elucidate the nature of the binding motifs, the strength of association, and the structural preferences that govern these ion pairs. This study not only contributes to the fundamental understanding of borate chemistry but also has potential implications for the design of advanced materials in ionic liquids, battery electrolytes, and coordination polymers.

COMPUTATIONAL METHODS

Geometry optimizations were performed using the ωB97M-V[11] (in Q-Chem6)[12] and M06-2X[13] (in Gaussian16)[14] functionals and the def2-TZVPD basis sets for all atoms, including the quasi-relativistic def2 electron core potentials for heavy atoms (Rb and Cs). The geometrical and energetic results are very similar for the two functionals (see the Supplementary Information for the ωB97M-V geometries and energies). All optimized structures were confirmed to be real

minima of the corresponding potential energy surfaces by diagonalization of the Hessian matrix. Decomposition of the interaction energy was carried out by means of the second generation ALMO-EDA method[15] as implemented in Q-Chem6,[12] at the M06-2X/def2-TZVPD and ωB97M-V/def2-TZVP levels with correction of the BSSE for the charge transfer term. Molecular electrostatic potential maps were generated with GaussView[16] on the corresponding 0.001 Å isosurfaces of the electron density.

For the analysis of interatomic interactions we use the newly developed penetration index.[17, 18] The penetration index for an A-B atom pair (p_{AB}) is defined as:

$$p_{AB} = 100 \cdot (v_A + v_B - d_{AB})/(v_A + v_B - r_A - r_B) \qquad \text{(Eq. 1)}$$

where d is the interatomic distance between atoms A and B, and r and v are the corresponding covalent[19] and van der Waals[20] radii, respectively. When two atoms lie at a separation equal to their summed van der Waals radii, the penetration index p_{AB} is 0%. As they move closer to a distance defined by the sum of their covalent radii, p_{AB} rises to 100%. For separations in between these two extremes, p_{AB} adopts intermediate values, reflecting weaker or noncovalent forms of interaction. Moreover, p_{AB} can adopt values over 100% for distances shorter than the sum of the covalent radii and under 0% for distances longer than the sum of the van de Waals radii. The use of this parameter offers several advantages over relying on simple interatomic distances because it provides a size-corrected, unified measure of how deeply two atoms' outer regions overlap regardless of their nature.[21, 22]

Despite based on covalent radii, penetration indices have been successfully used for the analysis of ionic solids, since the sum of cationic and anionic radii for atoms A and B yields a value that is very close to the sum of the corresponding covalent radii.[18, 23] In the present case, however, monoatomic ions interact with large counterions (namely TMB) which are held together via covalent bonds with the charge density distributed all around the molecule. Given the intermediate nature of these systems, we propose to evaluate the applicability of ionic radii for monoatomic ions as a means to account for the respective contraction and expansion of the electron cloud in cations and anions. Simultaneously, we retain the use of covalent radii for those atoms constituting the larger counterions. To this end, we compare the sum of the covalent radii of atoms A and B with the sum of the covalent radius of A and the ionic radius of B across a series of atom pairs pertinent to the systems under consideration (Figure1). Accordingly, we incorporate the ionic radii of Li, Na, K, Rb, and Cs.

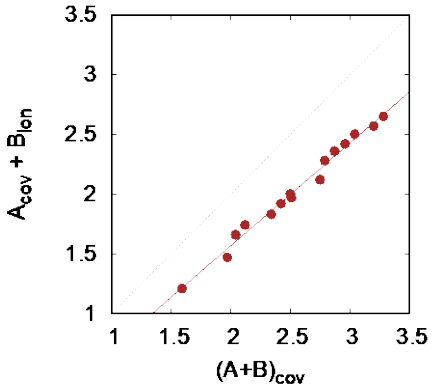

Figure 1. Correlation between the sum of the covalent radii of A and B and the sum of the covalent radius of A and the ionic radius of B, for TMB-alkali metal pairs (A = C, H, B; B = Li^+, Na^+, K^+, Rb^+, Cs^+).

$$[A_{cov} + B_{ion}] = 0.86\ [(A+B)_{cov}] - 0.15 \qquad \text{(Eq. 2)}$$

Figure 1 shows that, for monoatomic cations (alkali metals) interacting with C, H and B, there is a linear correlation between the sum of the covalent radii and the sum of the covalent and ionic radii. Interestingly, the straight line is displaced -0.15 Å with respect to that associated with the sum of only the covalent radii, while the slope is reduced to 0.86 (equation 2; $R^2 = 0.998$). In the light of these results, we assume that the use of the original formulation of the penetration index can correctly capture possible trends without having to combine covalent and ionic radii. Accordingly, all penetration indices throughout this article are calculated by means of Equation 1.

RESULTS AND DISCUSSION

First, in order to identify the molecular regions most likely to interact with an electrophile, we have represented the molecular electrostatic potential (MEP) of the tetramethylborate anion on its van der Waals isosurface. (Fig. 2). We have identified three points that represent minima of the electrostatic potential. Point **A** is a local minimum and is located at the extension of each of the C-B bonds (-99.9 kcal/mol). Point **B** is located between two methyl groups, at the center of one of the edges of the tetrahedral system, representing the most negative value of the EP in the entire molecule ($V_{s,min}$ = -111.6 kcal/mol). Finally, point **C** corresponds to another local minimum (-109.1 kcal/mol), located at the center of one of the tetrahedron's faces, and is therefore equidistant from three methyl groups.

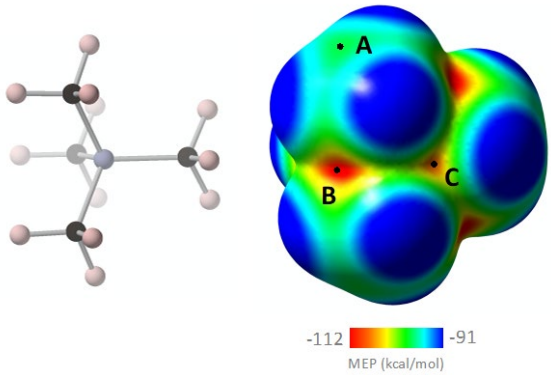

Figure 2. Chemical structure (left) and Molecular electrostatic potential (MEP) of tetramethylborate on the 0.001 Å^{-3} isodensity surface (right). Points **A** (-99.9 kcal/mol) and **C** (-109.1 kcal/mol) represent local minimum values of the EP while point **B** is the global minimum ($V_{s,min}$ = -111.6 kcal/mol).

According to our MEP map, interaction with monoatomic cations should be energetically favored at sites **A**, **B** and **C**. Each of these electrophilic regions might involve different interaction modes depending on the closeness to carbon and hydrogen atoms of the methyl groups (Chart 1).

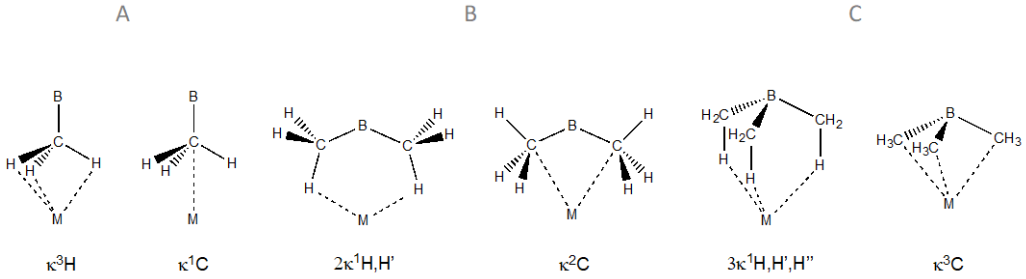

Chart 1. Possible interaction modes between tetramethylborate and a metallic cation involving regions **A**, **B** and **C** of the anion.

We next carried out geometry optimizations for ion pairs composed of TMB and a series of alkali metal cations (TMB···M; M = Li^+, Na^+, K^+, Rb^+, Cs^+). Exploration of the potential energy surface for each TMB–alkali metal combination revealed several energy minima, which are summarized in Table 1. As anticipated, three distinct interaction geometries were identified for each metal cation, corresponding to binding sites **A**, **B**, and **C**. The sole exception was observed for Cs^+, where structures initially corresponding to interaction topology **C** consistently relaxed to topology **B** upon optimization. This behavior is likely attributable to the large size of Cs^+, which hinders the stabilization of 3κ¹H,H′,H″ or κ³C interaction modes.

Analysis of the computed penetration indices (Table 1) allows for unambiguous assignment of the interaction mode adopted by each ion pair, as defined in Chart 1. For cations interacting via site **A**, the κ¹C mode predominates, characterized by substantial M···C penetration

values (103.0–107.5%) and moderately significant M···H ones (79.8–93.3%). In the case of site **B** interactions, the ion pairs are best described as κ^2C systems, with M···C penetration values (103.5–107.1%) comparable to those observed for site **A**, but with the addition of notable M···B peentrations (84.1–95.3%). Notably, for both **A** and **B** geometries, the degree of M···H penetration increases progressively down the alkali metal group.

In contrast, ion pairs adopting interaction site **C** exhibit a more intricate interaction pattern. Based on the calculated penetration indices, these interactions are best classified as κ^1B, displaying unexpectedly large M···B penetrations (99.5–108.4%). For Li^+, the corresponding M···H penetrations are relatively small, whereas for Na^+, K^+ and Rb^+, they become more prominent. In the case of Rb^+, M···H and M···B penetration values are particularly close, suggesting a nearly balanced interaction. It is also noteworthy that, for site **C** geometries, M···H penetration increases while M···B penetration decreases with increasing cation size.

Table 1. Main geometrical parameters calculated at the M06-2X/def2-TZVPD level for the adducts composed of tetramethylborate interacting with different metallic cations (M^+ = Li, Na, K, Rb, Cs) via **A**, **B** and **C** interacting sites.

M^+	Int. site	$P_{M\cdots C}$ (%)	$P_{M\cdots H}$ (%)	$p_{M\cdots B}$ (%)	Int. mode
Li	**A**	103.8	79.8	19.9	κ^1C
	B	105.4	76.9	95.3	κ^2C
	C	95.1	83.8	108.4	κ^1B (κ^3C)
Na	**A**	104.9	83.2	20.4	κ^1C
	B	105.4	84.4	90.1	κ^2C
	C	95.7	96.4	105.8	κ^1B (κ^3C)
K	**A**	104.1	84.9	14.1	κ^1C
	B	105.3	88.7	84.7	κ^2C
	C	94.1	96.8	102.8	κ^1B ($3\kappa^1$H,H',H'')
Rb	**A**	103.0	88.4	26.4	κ^1C
	B	103.5	91.6	84.1	κ^2C
	C	94.1	98.9	99.5	κ^1B ($3\kappa^1$H,H',H'')
Cs	**A**	107.5	93.3	32.2	κ^1C
	B	107.1	97.4	87.7	κ^2C

Focusing on systems in which the cation interacts via **C**, it is instructive to compare their behavior with previously reported tetramethylammonium–halide (TMA–halide) ion pairs.[24] In the latter, optimized geometries typically display low N–C–H tetrahedral angles in the range of 104–108°, consistent with relatively compact ion-pairing geometries. In contrast, systems involving TMB and alkali metal cations exhibit significantly wider B–C–H angles—reaching up to 124°—which facilitates notably short metal–boron (M···B) contacts compared to their TMA–halide counterparts (Figure 3). This structural trend is particularly striking given that the boron center in TMB carries a partial positive charge (see relevant NPA atomic charges in Table 2), which would

normally suggest a degree of electrostatic repulsion with the alkali metal cation. In fact, our analysis reveals a correlation: as the positive charge on the boron atom decreases, the M···B distance shortens, indicating deeper metal penetration into the boron center (Figure 4). We propose that any repulsive interaction between the boron and metal centers is effectively offset by three stabilizing interactions between the cation and the (partially) negatively charged carbon atoms. This arrangement bears resemblance to the concept of collective interactions,[25] wherein multiple weak attractive forces act cooperatively to stabilize otherwise unfavorable configurations (see Figure 3). Finally, the fact that atomic charges of H atoms are slightly positive can explain the absence of hydrogen bond-dominated topologies (k^3H, 2κ^{1}H,H′ and 3κ^{1}H,H′,H″) among the optimized systems (Table 1), also facilitating the establishment of M···C short contacts by opening the B-C-H angle.

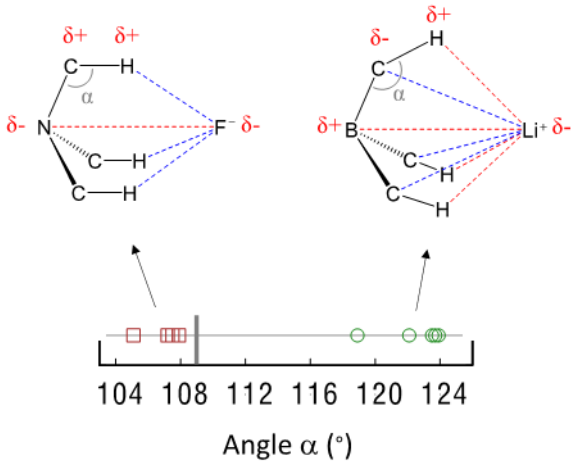

Figure 3. Angles α for tetramethylborate-alkali metal (green circles) and tetramethylammonium-halide (red squares) ion pairs. Values for the latter have been retrieved from geometry optimizations in ref. [21]. The grey bar represents the standard value of a tetrahedral angle.

Table 2. NPA atomic charges (q) for the adducts composed of tetramethylborate interacting with different metallic cations (M^+ = Li, Na, K, Rb, Cs) via **C**, calculated at the M06-2X/def2-TZVPD level.

M^+	q_C	q_H	q_B	q_M
Li	-0.87	+0.14	+0.11	+0.93
Na	-0.87	+0.13	+0.15	+0.97
K	-0.86	+0.13	+0.16	+0.98
Rb	-0.85	+0.12	+0.17	+0.98

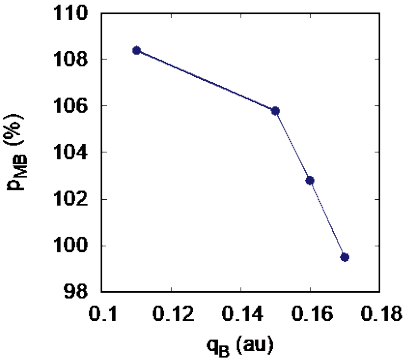

Figure 4. Dependence of the M···B penetration index with the atomic charge of B for the adducts composed of tetramethylborate interacting with different metallic cations (M^+ = Li, Na, K, Rb) via **C** interacting site.

Table 3. EDA terms with correction for the BSSE for the adducts composed of tetramethylborate interacting with different metallic cations (M^+ = Li, Na, K, Rb, Cs) via **A**, **B** and **C** interacting sites at the M06-2X/def2-TZVP level. The values in parenthesis represents the percentage of the term with respect to the sum of the total attractive energy. All energies are given in kcal mol^{-1}.

M^+	Int. site	ΔE_{elec}	ΔE_{Pauli}	ΔE_{disp}	ΔE_{pol}	ΔE_{CT}	ΔE_{INT}
Li	**A**	-110.9 (79.1)	22.4	-2.0 (1.4)	-20.9 (14.9)	-6.5 (4.7)	-117.9
	B	-129.4 (73.7)	29.6	-3.1 (1.7)	-36.1 (20.5)	-7.0 (4.0)	-145.9
	C	-133.9 (72.3)	31.8	-3.4 (1.8)	-39.9 (21.5)	-8.0 (4.3)	-153.5
Na	**A**	-102.6 (84.5)	19.8	-2.5 (2.1)	-14.8 (12.1)	-1.5 (1.2)	-101.6
	B	-117.8 (81.1)	24.2	-4.1 (2.8)	-21.7 (14.9)	-1.6 (1.1)	-120.9
	C	-123.7 (80.1)	27.8	-4.5 (2.9)	-24.0 (15.6)	-2.1 (1.4)	-126.6
K	**A**	-91.6 (85.1)	20.4	-3.3 (3.1)	-10.2 (9.5)	-2.5 (2.3)	-87.3
	B	-106.2 (80.8)	26.4	-5.9 (4.5)	-16.0 (12.2)	-3.3 (2.5)	-105.1
	C	-111.3 (79.8)	30.2	-6.5 (4.7)	-17.7 (12.7)	-4.0 (2.9)	-109.4
Rb	**A**	-86.8 (84.5)	19.9	-3.9 (3.8)	-8.7 (8.5)	-3.3 (3.2)	-82.8
	B	-100.1 (80.8)	25.0	-6.6 (5.4)	-14.2 (11.5)	-2.9 (2.3)	-98.9
	C	-104.6 (79.7)	28.6	-7.4 (5.6)	-15.7 (12.0)	-3.6 (2.7)	-102.6
Cs	**A**	-84.7 (81.9)	23.2	-4.8 (4.7)	-9.3 (9.02)	-4.5 (4.4)	-80.1
	B	-97.4 (78.4)	28.7	-8.1 (6.5)	-14.8 (11.9)	-3.9 (3.1)	-95.5

Table **3** shows the energy decomposition analysis (EDA) for the adducts composed of tetramethylborate interacting with different metallic cations (M^+ = Li, Na, K, Rb, Cs) via **A**, **B** and **C** interacting sites. In general, the calculated interaction energies (ΔE_{INT}) are significantly large (between -80.1 and -153.3 kcal mol^{-1}), as expected for ion pairs. The interaction energy decreases progressively down the alkali metal group for all three interaction sites. Among these, site **C** exhibits the strongest interaction, whereas site **A** corresponds to the weakest. The electrostatic term (ΔE_{elec}) dominates the cohesive forces comprising 72-3 – 85.1% of the total attractive energy. Polarization (ΔE_{pol}) represents the second most significant energetic contribution. Its relative importance increases in the order **A** < **B** < **C**, with corresponding percentage contributions ranging from 9.0–14.9% for **A**, 11.9–20.5% for **B**, and 12.7–21.5% for **C**. Across the series of alkali metal cations, the ΔE_{pol} contribution decreases progressively when descending the group. Finally, dispersion (ΔE_{disp}) and charge transfer (ΔE_{CT}) represent only a small fraction of the total attractive energy (1.4 – 7.3% for ΔE_{disp} and 1.2 – 4.7% for ΔE_{CT}).

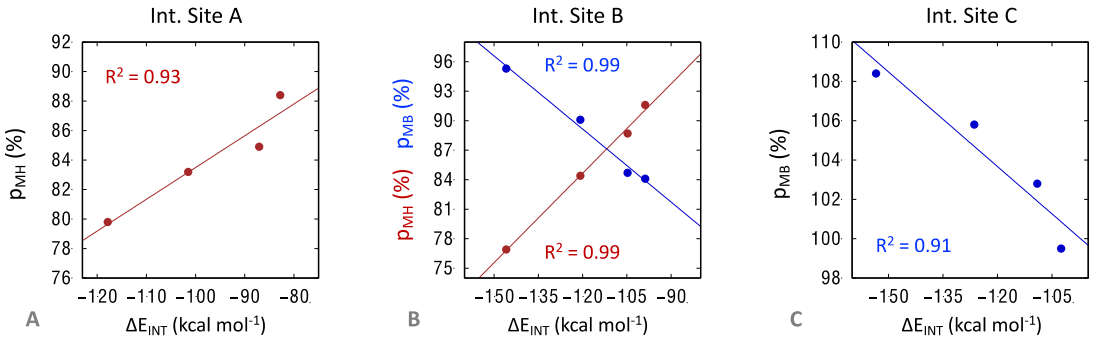

Figure 5. Linear correlations between interaction energies and relevant penetration indices, namely p_{MH} (red) and p_{MB} (blue) for the adducts composed of tetramethylborate interacting with different alkali metal cations (M^+ = Li, Na, K, Rb) via **A**, **B** and **C** interacting sites.

For the systems under study, we have also discovered some intriguing relationships between the interaction energy and various penetration indices involving the alkali metal cations. For ion pairs interacting via **A**, the interaction energy depends linearly on the MH penetration index: the larger the M···H penetration, the weaker the TMB···M interaction (Fig. 5A). This is in good agreement with the δ+ character of the alkyl hydrogens, since even though the systems interacting through **A** show a κ^1C type interaction mode, the M···H penetrations are in all cases greater than 80%. Regarding the M···H penetration and its relationship to interaction energy, the **B** systems show a similar trend to the **A** series (Fig. 5B). Furthermore, there is a distinct linear correlation between the interaction energy and the M–B penetration, with increasing p_{MB} values indicating interactions that become more stabilizing (Fig. 5B). This latter behavior is also found for systems interacting via **C** (Fig. 5C), although the B central atom shows a slightly positive

atomic charge. However, it must be noted that despite these positive atomic charges, the electrostatic potential is negative all around the molecule on the vdW surface, as it was shown in Fig. 2. Interestingly, no correlation between the interaction energy and the M···C penetration has been found for any interaction site.

CONCLUSIONS

In this work, we have investigated the interaction between the tetramethylborate anion (TMB) and a series of alkali metal cations (Li^+, Na^+, K^+, Rb^+, Cs^+) using molecular electrostatic potential (MEP) analysis, geometry optimizations, and energy decomposition analysis (EDA). The MEP surface of TMB revealed three distinct electrophilic regions (**A**, **B**, and **C**) corresponding to local and global minima in the electrostatic potential, which were used to define different cation-binding topologies. Optimization of the TMB···M^+ ion pairs revealed several stable interaction geometries, with three characteristic coordination modes (κ^1C, κ^2C, and κ^1B) identified across the series. Notably, deeper M···B penetration was observed in geometries involving interaction site **C**, despite the boron center bearing a partial positive charge. This seemingly counterintuitive result is rationalized through the concept of collective interactions, wherein stabilizing M···C contacts compensate for electrostatic repulsion at the boron center.

Penetration indices provided a reliable metric for classifying interaction modes and understanding the structural trends observed upon descending the alkali metal group. The interaction strength generally decreased from Li^+ to Cs^+ and followed the trend **C** > **B** > **A**, reflecting not only the increasing size and decreasing charge density of the cations, but also the varying geometrical accessibility of the interaction sites. EDA results confirmed that electrostatics dominate the attractive forces, while polarization contributions become increasingly important in stronger interaction modes. Dispersion and charge-transfer effects, although present, play a relatively minor role.

Finally, we uncovered linear correlations between interaction energies and M···H and M···B penetration indices in topologies **A**, **B**, and **C**. These trends underscore the importance of non-covalent contacts involving hydrogen and boron in modulating the overall stability of the ion pairs. Our findings provide valuable insight into the structural and energetic features governing cation–anion interactions involving sterically hindered borate anions and may serve as a foundation for understanding similar systems in coordination chemistry, ionic liquids, and molecular design.

Data availability

The data supporting this article have been included as part of the ESI.

Conflicts of interests

There are no conflicts to declare.

Acknowledgements

This work was supported by projects PID2022-140244NB-I00 and PID2021-122763NB-I00, funded by MCIN/AEI/10.13039/501100011033 and by "ESF Investing in your future". Technical support from the Instituto de Biocomputación y Física de Sistemas Complejos (Universidad de Zaragoza) is also acknowledged.

REFERENCES

(1) Umebayashi, Y.; Han, J.; Watanabe, H., Toward New Ion Conductive Liquids via Ionic Liquids. *The Chemical Record* **2023,** 23, e202200302.
(2) Si, H.; Ma, J.; Xia, X.; Wang, Q.; Geng, S.; Fu, L., Solid-State Sodium-Ion Batteries: Theories, Challenges and Perspectives. *Chemistry – A European Journal* **2025,** 31, e202403247.
(3) Yu, B.; Pettitt, B. M.; Iwahara, J., Dynamics of Ionic Interactions at Protein–Nucleic Acid Interfaces. *Acc. Chem. Res.* **2020,** 53, 1802-1810.
(4) Mele, A.; Tran, C. D.; De Paoli Lacerda, S. H., The Structure of a Room-Temperature Ionic Liquid with and without Trace Amounts of Water: The Role of C□H···O and C-H···F Interactions in 1-n-Butyl-3-Methylimidazolium Tetrafluoroborate. *Angew. Chem. Int. Ed.* **2003,** 42, 4364-4366.
(5) Zhu, D.; Kochi, J. K., Alkylation of Pyridinium Acceptors via Thermal and Photoinduced Electron Transfer in Charge-Transfer Salts with Organoborates. *Organometallics* **1999,** 18, 161-172.
(6) Altalhi, W. A. O.; Chan, B.; O'Hair, R. A. J., Methide Affinity Scale: Key Thermodynamic Data Underpinning Catalysis, Organic Synthesis, and Organometallic and Polymer Chemistry. *J. Phys. Chem. A* **2024,** 128, 977-988.
(7) Sieradzan, I.; Anusiewicz, I., The electronic stability decrease in the BF4–n(R)n-anions (R=CH3, C2H5; n=0–4). *Chem. Phys.* **2013,** 425, 55-61.
(8) Freire, M. G.; Neves, C. M. S. S.; Marrucho, I. M.; Coutinho, J. A. P.; Fernandes, A. M., Hydrolysis of Tetrafluoroborate and Hexafluorophosphate Counter Ions in Imidazolium-Based Ionic Liquids. *J. Phys. Chem. A* **2010,** 114, 3744-3749.
(9) Mohtadi, R.; Matsui, M.; Arthur, T. S.; Hwang, S.-J., Magnesium Borohydride: From Hydrogen Storage to Magnesium Battery. *Angew. Chem. Int. Ed.* **2012,** 51, 9780-9783.
(10) Cushion, M. G.; Mountford, P., Cationic and charge-neutral calcium tetrahydroborate complexes and their use in the controlled ring-opening polymerisation of rac-lactide. *Chem. Commun.* **2011,** 47, 2276-2278.
(11) Mardirossian, N.; Head-Gordon, M., ωB97M-V: A combinatorially optimized, range-separated hybrid, meta-GGA density functional with VV10 nonlocal correlation. *The Journal of Chemical Physics* **2016,** 144.
(12) Epifanovsky, E.; Gilbert, A. T. B.; Feng, X.; Lee, J.; Mao, Y.; Mardirossian, N.; Pokhilko, P.; White, A. F.; Coons, M. P.; Dempwolff, A. L.; Gan, Z.; Hait, D.; Horn, P. R.; Jacobson, L. D.; Kaliman, I.; Kussmann, J.; Lange, A. W.; Lao, K. U.; Levine, D. S.; Liu, J.;

McKenzie, S. C.; Morrison, A. F.; Nanda, K. D.; Plasser, F.; Rehn, D. R.; Vidal, M. L.; You, Z.-Q.; Zhu, Y.; Alam, B.; Albrecht, B. J.; Aldossary, A.; Alguire, E.; Andersen, J. H.; Athavale, V.; Barton, D.; Begam, K.; Behn, A.; Bellonzi, N.; Bernard, Y. A.; Berquist, E. J.; Burton, H. G. A.; Carreras, A.; Carter-Fenk, K.; Chakraborty, R.; Chien, A. D.; Closser, K. D.; Cofer-Shabica, V.; Dasgupta, S.; de Wergifosse, M.; Deng, J.; Diedenhofen, M.; Do, H.; Ehlert, S.; Fang, P.-T.; Fatehi, S.; Feng, Q.; Friedhoff, T.; Gayvert, J.; Ge, Q.; Gidofalvi, G.; Goldey, M.; Gomes, J.; González-Espinoza, C. E.; Gulania, S.; Gunina, A. O.; Hanson-Heine, M. W. D.; Harbach, P. H. P.; Hauser, A.; Herbst, M. F.; Hernández Vera, M.; Hodecker, M.; Holden, Z. C.; Houck, S.; Huang, X.; Hui, K.; Huynh, B. C.; Ivanov, M.; Jász, Á.; Ji, H.; Jiang, H.; Kaduk, B.; Kähler, S.; Khistyaev, K.; Kim, J.; Kis, G.; Klunzinger, P.; Koczor-Benda, Z.; Koh, J. H.; Kosenkov, D.; Koulias, L.; Kowalczyk, T.; Krauter, C. M.; Kue, K.; Kunitsa, A.; Kus, T.; Ladjánszki, I.; Landau, A.; Lawler, K. V.; Lefrancois, D.; Lehtola, S.; Li, R. R.; Li, Y.-P.; Liang, J.; Liebenthal, M.; Lin, H.-H.; Lin, Y.-S.; Liu, F.; Liu, K.-Y.; Loipersberger, M.; Luenser, A.; Manjanath, A.; Manohar, P.; Mansoor, E.; Manzer, S. F.; Mao, S.-P.; Marenich, A. V.; Markovich, T.; Mason, S.; Maurer, S. A.; McLaughlin, P. F.; Menger, M. F. S. J.; Mewes, J.-M.; Mewes, S. A.; Morgante, P.; Mullinax, J. W.; Oosterbaan, K. J.; Paran, G.; Paul, A. C.; Paul, S. K.; Pavošević, F.; Pei, Z.; Prager, S.; Proynov, E. I.; Rák, Á.; Ramos-Cordoba, E.; Rana, B.; Rask, A. E.; Rettig, A.; Richard, R. M.; Rob, F.; Rossomme, E.; Scheele, T.; Scheurer, M.; Schneider, M.; Sergueev, N.; Sharada, S. M.; Skomorowski, W.; Small, D. W.; Stein, C. J.; Su, Y.-C.; Sundstrom, E. J.; Tao, Z.; Thirman, J.; Tornai, G. J.; Tsuchimochi, T.; Tubman, N. M.; Veccham, S. P.; Vydrov, O.; Wenzel, J.; Witte, J.; Yamada, A.; Yao, K.; Yeganeh, S.; Yost, S. R.; Zech, A.; Zhang, I. Y.; Zhang, X.; Zhang, Y.; Zuev, D.; Aspuru-Guzik, A.; Bell, A. T.; Besley, N. A.; Bravaya, K. B.; Brooks, B. R.; Casanova, D.; Chai, J.-D.; Coriani, S.; Cramer, C. J.; Cserey, G.; DePrince, A. E., III; DiStasio, R. A., Jr.; Dreuw, A.; Dunietz, B. D.; Furlani, T. R.; Goddard, W. A., III; Hammes-Schiffer, S.; Head-Gordon, T.; Hehre, W. J.; Hsu, C.-P.; Jagau, T.-C.; Jung, Y.; Klamt, A.; Kong, J.; Lambrecht, D. S.; Liang, W.; Mayhall, N. J.; McCurdy, C. W.; Neaton, J. B.; Ochsenfeld, C.; Parkhill, J. A.; Peverati, R.; Rassolov, V. A.; Shao, Y.; Slipchenko, L. V.; Stauch, T.; Steele, R. P.; Subotnik, J. E.; Thom, A. J. W.; Tkatchenko, A.; Truhlar, D. G.; Van Voorhis, T.; Wesolowski, T. A.; Whaley, K. B.; Woodcock, H. L., III; Zimmerman, P. M.; Faraji, S.; Gill, P. M. W.; Head-Gordon, M.; Herbert, J. M.; Krylov, A. I., Software for the frontiers of quantum chemistry: An overview of developments in the Q-Chem 5 package. *The Journal of Chemical Physics* **2021,** 155.

(13) Zhao, Y.; Truhlar, D. G., The M06 suite of density functionals for main group thermochemistry, thermochemical kinetics, noncovalent interactions, excited states, and transition elements: two new functionals and systematic testing of four M06-class functionals and 12 other functionals. *Theor. Chem. Acc.* **2008,** 120, 215-241.

(14) Gaussian 16, Revision B.01, Frisch, M. J.; Trucks, G. W.; Schlegel, H. B.; Scuseria, G. E.; Robb, M. A.; Cheeseman, J. R.; Scalmani, G.; Barone, V.; Petersson, G. A.; Nakatsuji, H.; Li, X.; Caricato, M.; Marenich, A. V.; Bloino, J.; Janesko, B. G.; Gomperts, R.; Mennucci, B.; Hratchian, H. P.; Ortiz, J. V.; Izmaylov, A. F.; Sonnenberg, J. L.; Williams-Young, D.; Ding, F.; Lipparini, F.; Egidi, F.; Goings, J.; Peng, B.; Petrone, A.; Henderson, T.; Ranasinghe, D.; Zakrzewski, V. G.; Gao, J.; Rega, N.; Zheng, G.; Liang, W.; Hada, M.; Ehara, M.; Toyota, K.; Fukuda, R.; Hasegawa, J.; Ishida, M.; Nakajima, T.; Honda, Y.; Kitao, O.; Nakai, H.; Vreven, T.; Throssell, K.; Montgomery, J. A., Jr.; Peralta, J. E.; Ogliaro, F.; Bearpark, M. J.; Heyd, J. J.; Brothers, E. N.; Kudin, K. N.; Staroverov, V. N.; Keith, T. A.; Kobayashi, R.; Normand, J.; Raghavachari, K.; Rendell, A. P.; Burant, J. C.; Iyengar, S. S.;

Tomasi, J.; Cossi, M.; Millam, J. M.; Klene, M.; Adamo, C.; Cammi, R.; Ochterski, J. W.; Martin, R. L.; Morokuma, K.; Farkas, O.; Foresman, J. B.; Fox, D. J. Gaussian, Inc., Wallingford CT, 2016.
(15) Horn, P. R.; Mao, Y.; Head-Gordon, M., Probing non-covalent interactions with a second generation energy decomposition analysis using absolutely localized molecular orbitals. *Phys. Chem. Chem. Phys.* **2016,** 18, 23067-23079.
(16) *GaussView, version 5, R. Dennington, T. Keith and J. Millam, Semichem Inc., Shawnee Mission, KS, 2009.* . ed.
(17) Gil, D. M.; Echeverría, J.; Alvarez, S., Tetramethylammonium Cation: Directionality and Covalency in Its Interactions with Halide Ions. *Inorg. Chem.* **2022,** 61, 9082-9095.
(18) Echeverría, J.; Alvarez, S., The borderless world of chemical bonding across the van der Waals crust and the valence region. *Chemical Science* **2023,** 14, 11647-11688.
(19) Cordero, B.; Gómez, V.; Platero-Prats, A. E.; Revés, M.; Echeverría, J.; Cremades, E.; Barragán, F.; Alvarez, S., Covalent radii revisited. *Dalton Transactions* **2008**, 2832-2838.
(20) Alvarez, S., A cartography of the van der Waals territories. *Dalton Transactions* **2013,** 42, 8617-8636.
(21) Echeverría, J.; Alvarez, S., Widening the Scope of Structural Correlations by Means of the van der Waals Crust Penetration Indices: The Dimerization of Groups 11 and 12 L–M–X Halo Complexes. *Crystal Growth & Design* **2024,** 24, 4743-4747.
(22) Velasquez, J. D.; Keshtkar, N.; Polo, V.; Munárriz, J.; Echeverría, J., Unveiling the Potential of Haloalkenes as Electron Density Acceptors. *Crystal Growth & Design* **2024,** 24, 5775-5780.
(23) Echeverría, J.; Alvarez, S., The Interpenetration Index and Its Applications in Chemistry. In Springer Berlin Heidelberg: Berlin, Heidelberg, pp 1-34.
(24) Gil, D. M.; Echeverría, J.; Alvarez, S., Tetramethylammonium Cation: Directionality and Covalency in Its Interactions with Halide Ions. *Inorganic Chemistry* **2022,** 61, 9082-9095.
(25) Sowlati-Hashjin, S.; Šadek, V.; Sadjadi, S.; Karttunen, M.; Martín-Pendás, A.; Foroutan-Nejad, C., Collective interactions among organometallics are exotic bonds hidden on lab shelves. *Nature Communications* **2022,** 13, 2069.